FILM SIDE LASER PATTERNING OF MOLYBDENUM THIN FILMS SPUTTER-DEPOSITED ONTO GLASS

C. Schultz[1], M. Schüle[1], K. Stelmaszczyk[1], J. Bonse[2], R. Witteck[1], M.Weizman[1], H. Rhein[1]
B. Rau[3], R. Schlatmann[1,3], V. Quaschning[1], B. Stegemann[1] , F. Fink[1]

[1] *HTW Berlin - University of Applied Sciences, Wilhelminenhofstr. 75a, 12459 Berlin, Germany*
[2] *BAM Bundesanstalt für Materialforschung und –prüfung, Unter den Eichen 87, 12205 Berlin, Germany*
[3] *PVcomB - Helmholtz-Zentrum Berlin für Materialien und Energie GmbH, Schwarzschildstr. 3, D-12489 Berlin, Germany*

ABSTRACT: Serial interconnection of CIGSe thin film solar modules involves typically glass-side laser patterning of the molybdenum layer (P1 scribe). In this paper we present a working principle of P1 film side patterning. The investigated samples were sputter-deposited onto soda-lime glass substrates. For understanding the fundamental ablation behavior, two kinds of layer systems were studied: on the one hand monolayer systems which are compressively stressed and on the other hand bilayer systems, consisting of a tensile stressed layer on the substrate and a second layer on top. The film-side ablation process was studied using a nanosecond as well as a picosecond laser source. The influence of intrinsic stress was studied by XRD. Time resolved spectroscopy reveals the formation of plasma as important driving mechanism for ablation. It is shown that by proper adaption of the sputter conditions high-quality P1 film side patterning is achieved.
Keywords: Laser Processing, Molybdenum, Strain, Ablation, Sputter Deposition, Cu(InGa)Se_2

1 INTRODUCTION

Economically viable photovoltaic (PV) power generation requires low-cost solar cells. Thin-film PV cells are being developed as a mean of substantially reducing material and energy consumption costs during manufacture. A thin film PV module consists of an active layer sandwiched between two electrically conductive layers on a substrate, typically glass. Various thin film technologies exist, which differ mainly in the type of absorber material. Commonly used are hydrogenated amorphous and microcrystalline silicon (e.g. a-Si:H/µc-Si:H tandem structures) or polycrystalline compounds like $Cu(In_x,Ga_{1-x})(Se_y,S_{1-y})_2$, i.e. CIGSe, and CdTe.

Structuring the module into a number of serially interconnected cells is necessary in order to limit the current and to increase the voltage. This structuring involves the complete and selective ablation of very fine lines within the thin film layers to form serial interconnections between the front and back contact while electrically isolating the individual solar cells. As shown in Fig. 1(a), three scribing steps P1, P2, and P3 alternating with layer deposition are necessary to separate the solar cells and to perform so-called monolithic interconnection.

At present, most of the fabricated chalcopyrite based solar cells are deposited onto glass substrates where the high quality and the high stability of the glass side patterning process is well established. In contrast to glass side patterning of thin metal layers, film side patterning often leads to undesirable scribing results and is thus disadvantageous [1]. Here we demonstrate that high quality film side patterning onto glass is possible just by adapting the sputter process and making of internal stress. This advantageous, so-called post pulse ablation behavior will be adapted and could be also used for applications onto flexible substrates.

Typically, in industrial production of thin film solar modules three patterning steps are performed for monolithical interconnection. In this work the patterning step P1 is investigated. Further details for alternative P2 and P3 patterning can be found in [2]. Presently, in the case of CIGSe module manufacturing the patterning of the back contact by laser is well established and in most cases for the sputter-deposited molybdenum a broad processing window is found [3]. In the case of film side molybdenum patterning the success of the back contact patterning depends strongly on the physical and mechanical layer properties due to varying sputter conditions [4]. Scofield et al. [4] investigated already the molybdenum bilayer stack as back contact for chalcopyrite solar cells and found that it is advantageous with respect to layer adhesion and electrical conductivity. In that work it was found that tensile stressed intermediate layers are responsible for good adhesion. In contrast, compact and dense layers deposited at low sputter gas pressures are worse in adhesion, whereas the compact microstructure enhances the conductivity, leading to low electrical sheet resistances.

Combining both layers provides good mechanical adhesion as well as desirable electric properties of the Mo-layer. While glass-side patterning of Mo bilayers is well-established, the challenge of this study is to adapt all processing steps for creating a film side pattern and thus to enable high quality scribing results on opaque substrates.

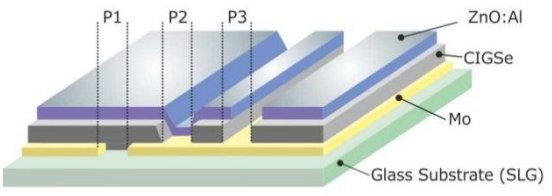

Figure 1: Schematics of monolithically inter-connected CIGSe thin film solar cell with P1, P2 and P3 scribes to electrically isolate adjacent cells.

It is well known [5] that tight focusing, in order to keep the area losses small, can lead to undesirable Mo ridges which can generate shunts in the following processing steps. Our novel approach shows that for avoiding these ridges it is possible to adapt a post-pulse ablation mechanism which works like the direct induced ablation although the patterning is done from the film side.

2 EXPERIMENTAL

For laser structuring a high-speed motion system for high-precision laser processing (Rofin Baasel Lasertech) was available. This system consists of high-precision linear motor drives for x-y-stages which can be precisely moved at a speed of up to 1.2 m/s.

For laser structuring with nanosecond pulses the "SL 3 SHG PV" (Rofin Baasel Lasertech) was used operating at 532 nm and 2 W maximum. The laser is a Q-switched, diode-pumped solid state laser with a pulse-to-pulse energy stability better than 1.5 %. The laser pulse duration was less than 13 ns and depends on the laser pulse repetition rate with a maximum of 400 kHz. For patterning with picosecond pulses a Time Bandwidth source was used, emitting 1064 nm as well as the frequency-doubled and tripled wavelengths with maximum pulse durations of about 10 ps. The maximum power of 15 W can be achieved for infrared radiation while the range of the repetition rate varies from 50 kHz up to 8.2 MHz. Both lasers were characterized as beams spatially Gaussian intensity distribution.

The molybdenum samples were prepared and studied at the Helmholtz-Zentrum Berlin (HZB) and the new facilities of the Competence Center for Thin-Film and Nanotechnology for Photovoltaics Berlin (PVcomB). The samples under investigation are composed as follows: 1.9 mm soda lime glass (SLG) substrate / 500 nm or 1000 nm Mo deposited at low argon pressure for monolayer samples. Bilayer samples are composed as: 1.9 mm soda lime glass (SLG) substrate / 200 nm Mo deposited at high argon pressure (providing a tensile stressed bottom Mo layer) and additional 300 nm or 800 nm Mo layer deposited at low argon pressure like the monolayer samples, see Table 1. Furthermore, for studying the behavior of each separated layer, both, a single tensile stressed as well as a single compressively stressed layer were deposited on the same SLG substrates. The thickness of these layers was the same as the thickness of the first layer in bilayer systems.

For characterization and analysis of the results of the laser treatment different techniques were applied including: optical microscopy (Carl Zeiss Axio Scope A1,) and scanning electron microscopy (SEM, Hitachi S4100). Electrical properties were elucidated by four point probe conductivity measurements (Jandel RM3-AR). For analyzing the internal stress, a PANalytical X-Pert Pro X-Ray Diffraction (XRD) tool was used to measure the peak shift and deriving the strain within the samples layers.

Table 1: The table summarized experimental parameters of the samples under investigation, i.e., their thickness, the deposition Argon pressure, and the intrinsic stress (derived from XRD measurements)

Sample Type	Mo layer thickness [nm]	Sputter pressure [µbar]	Intrinsic Stress [GPa]
200 nm monolayer tensile stress	200	20	0.598
200 nm monolayer compressive stress	200	4	-3.005
500 nm bilayer	200+300	20+4	-1.615
500 nm Monolayer	500	4	-0.93
1000 nm Bilayer	200+800	20+4	-1.247
1000 nm Monolayer	1000	4	-1.713

3 ANALYSIS OF THRESHOLD FLUENCES

Determining the threshold fluences for the samples under investigation were performed from both patterning sides. It allows a comparison of different samples within the experimental setup. Moreover, it gives as a result the threshold fluence as well as the Gaussian beam radii (ω_0^2) of the laser beam used for material processing. The method was first described by Liu [6] and holds true for (ideal) Gaussian beams applied from film side. The formula describes the squared ablated crater diameter (D^2) as function of the Gaussian beam radius (w_0) and in relation to the laser pulse energy (E_p) ratio to the threshold energy ($E_{p,th}$).

$$D^2(E_P) = 2\omega_0^2 \ln\left(\frac{E_P}{E_{P,th}}\right)$$

Using this method for glass side patterning an adaptation of the equation above has to be considered [7].

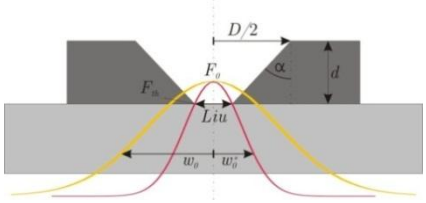

Figure 2: Geometrical considerations for adapting Liu´s method [6] for glass side patterning.

$$D^2(E_P) = 2\omega_0^2 \ln\left(\frac{E_P}{E_{P,th}}\right) + 2d * \tan(\alpha)$$

The experimental results shown in this paper are reduced here in order to keep it concise. Therefore, only results obtained at 532 nm wavelength and with ps- and ns-pulse

durations are presented in the following. The results for 1064 nm wavelength are qualitatively similar.

The plots of the glass side ablation threshold for both pulse regimes are subsequently shown in Figs. 3 and 4. In the case of ns-laser patterning (Fig. 3), the slope of all fitted curves is comparable as it was expected from the ablation model proposed by Liu [6]. The differences in the ablation threshold energy can be explained by varying adhesion of the different films to the substrate.

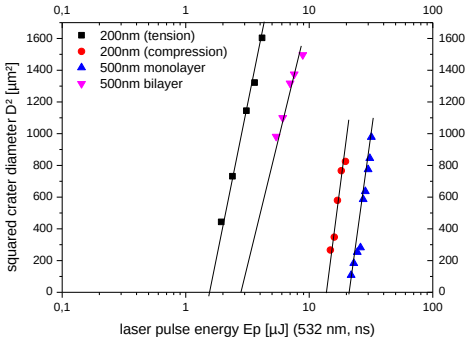

Figure 3: Squared crater diameter as function of the laser pulse energy for 532 nm, ns-laser pulses, glass side scribing geometry.

Moreover, it can be seen in Figure 3, that there are two groups of samples, corresponding on the one hand to the microstructure (adhesion) and on the other hand to the optical properties (reflectivity / energy coupling at the substrate- Mo-layer interface) both due to the different conditions during sputter deposition.
As it can be seen in Figure 4, the shorter ps-pulse duration leads to significantly reduced ablation threshold energies compared to the ns-case. This is caused by the reduced heat flow into the surrounding during the ps-pulses leading to an energy confinement here. Furthermore, it can be seen that there still exists a well pronounced offset in ablation energy for compressively stressed samples, what might be indicating that inner stresses or adhesion can differ between both samples despite the similar deposition conditions.

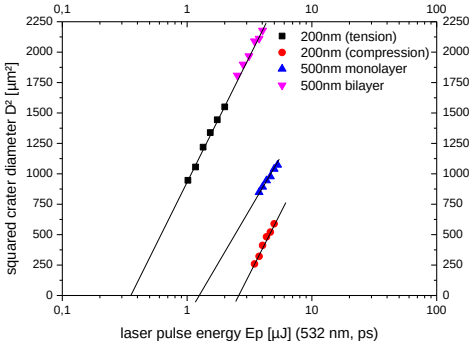

Figure 4: Squared crater diameter as function of the laser pulse energy for 532 nm, ps-laser pulses, glass side scribing geometry.

In contrast to the results shown above, film side patterning requires significantly higher laser pulse energies for patterning of the same samples. For compressively stressed samples the available pulse energies for ps-laser pulses were too low for reaching ablation of the deposited stack. Therefore, just the samples consisting of a tensile stressed layer can be compared with those of the glass side patterned in ps-range.

In the case of ns-laser patterning the dependency of the threshold fluence from the microstructure / inner strain build up two groups, similar to the glass side patterning results, see Figure 5. It should be noted that the threshold fluences are also very close to each other in this pulse duration regime. In the case of ps-laser patterning it can be seen that both datasets follow the behavior for Gaussian beams, indicating the same threshold, thus suggesting that the tensile stressed layer (1st layer) dominates the overall ablation mechanism of the stack. This behavior should be pointed out, because in the ps-laser patterning from the film side it would be expected that the ablation threshold increases with the thickness of the stack if the film thickness is smaller than the thermal penetration depth. Here, in this case for ps-laser patterning both samples (of different thickness but the same substrate-layer interface) shows the same behavior, indicating that the ablation starts after the laser pulse is applied. Therefore this mechanism is called “post pulse ablation”. It is pointed out that the optical patterning results for film- and glass side processing are similar for bilayer systems.

The film side laser processing at bilayer systems is a promising approach for achieving low cost flexible solar cells. Therefore, this ablation mechanism is investigated in more detail by complementary experimental techniques.

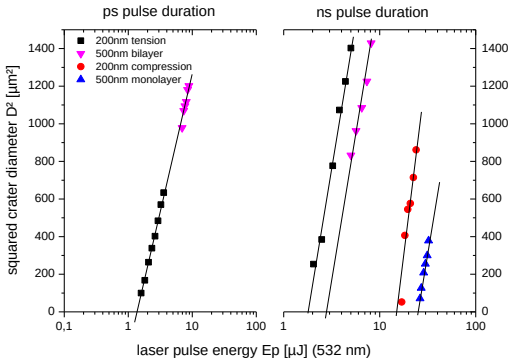

Figure 5: Comparison of the squared crater diameter as function of the laser pulse energy for 532 nm, ns- and ps-laser pulses, film side scribing geometry.

4 ELECTRICAL AND STRUCTURAL ANALYSIS

From the electrical point of view the lowest sheet resistance possible for the back contact application is desired. It is known [5] that in sputter deposited layers high mechanical stresses can occur resulting in cracks etc. for tensile stressed films. These cracks are responsible for high sheet resistances whereas compressively stressed films show very low sheet resistances due to large grains and less crystallographic defects. As mentioned above, for manufacturing of solar cells, both, a low sheet resistance and a good adhesion are advantageous. Therefore, the bilayer system was established to enable both features.

Figure 6 shows the electrical sheet resistance as a function of the total layer thickness for both the mono- and the bilayer systems (results on adhesion are not shown here). Significant differences are visible only for layer thicknesses < 250 nm. For such thin layers, the monolayer exhibits values ~ 7-times smaller than that of the bilayers.

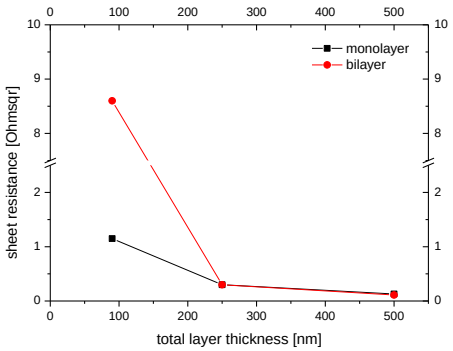

Figure 6: Dependency of the measured sheet resistance as function of the total Mo-layer thickness.

For the determination of mechanical strain in the Mo-films X-ray diffraction measurement were performed. It is known [8] that high inert gas pressures (i.e. 20 µbar Argon) during sputter deposition are leading to intrinsic tensile stress due to scattering of the sputter ions with the inert gas during the deposition process. On the other hand, low inert gas pressures (i.e. 4 µbar) are resulting in compressively stressed films due to the high kinetic energy of the target ions. Besides the strain resulting from the sputter conditions thermal strain may play a role, although in most cases for sputter deposited films it can be neglected. Thermal strain results from the different linear expansion coefficients of the stacked materials under varying temperatures upon cooling the samples from the deposition temperatures down to room temperature.

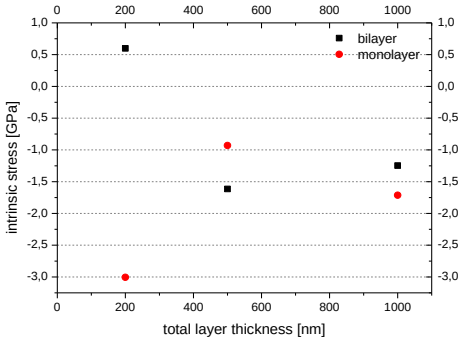

Figure 7: Intrinsic stress as function of the total film thickness for the two different layer types. The stress is derived from XRD-measurements.

The intrinsic stress is shown in Figure 7 as function of the layer thickness. It might be suggested that with increasing thickness of the film/stack the intrinsic stress converges to a certain saturation value between -1.0 to -1.5 GPa where the intrinsic mechanical stress in the Mo-layers becomes independent of the layer thickness.

In Figure 8 the peak positions for tensile stressed as well as for compressively stressed layers in comparison to the relaxed peak position of a powder reference sample (dashed vertical line) are shown. The peak positions (110 peak) for both samples show the expected behavior, supporting that the Bragg-condition holds true.

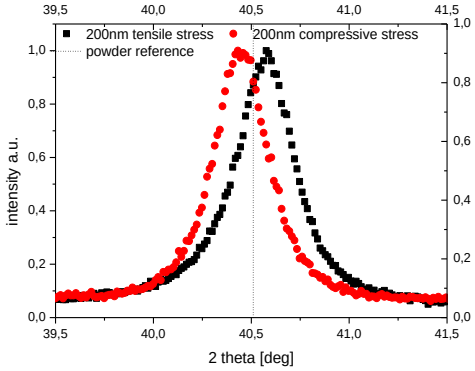

Figure 8: Displacement of the XRD rocking curve peaks for tensile and compressively stressed Mo-film samples of 200 nm thickness in comparison to the relaxed powder is shown.

5 TIME RESOLVED PLASMA SPECTROSCOPY

For gaining more details of the film side "post pulse ablation" mechanism, time resolved spectroscopy have been applied. For soda-lime glasses it is well known that these glasses consists of different constituents, among others Na_2O, Al_2O_3, CaO etc., thus it could be suggested that these components, excited by the laser beam, build up ions increasing the pressure contributing to the delamination of the molybdenum stack. In Figure 9 the relative Na concentration is shown as measured for different types of the stacks, using the spectroscopic setup described earlier. Note that the gain parameter of the ICCD camera and its integration time were kept constant throughout the measurements such that the relative difference in the intensity of the emission indicates the change of the Na concentration.

It can be seen that bilayer systems accommodate the highest content of Na, most likely due to diffusion from the glass in the molybdenum. The higher concentration in bilayer systems as compared to monolayer systems could be explained by their less dense microstructure. To prove that the higher content in bilayer systems results from diffusion further experiments should be performed.

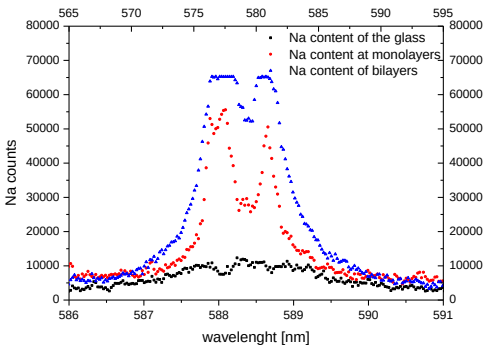

Figure 9: The Na content of the pure soda-lime glass, as well as the content of both layer types is shown.

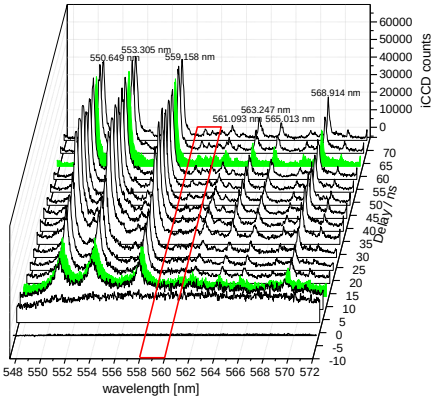

Figure 10: Temporal and spectral evolution of the Mo-glass interface plasma.

The temporal and spectral evolution of the Mo-glass interface plasma is shown in Figure 10, while 0 delay corresponds to the expected maximum of the laser pulse arriving at the sample. The strongest emission lines of Mo I are indicated behind the curves. The red area marks the region of spectral signature of the glass substrate, not verified as Mo emission. These additional emission lines were proven to result from the excitation of SLG constituents and are typically good indicators of the thermal melting of the glass substrate. As confirmed by the spectra registered at time delays of -5 and 0 ns this melting is most likely caused by the generation of hot, thermal plasma as indicated by the black-body continuum emission. The subsequent excitation and emission of characteristic Mo and SLG lines, clearly visible in Figure 10, suggest the expansion of ablated material and it's cooling on the ns time scale. The laser initiated spectra of the interface plasma registered at delays 10 ns and 60 ns are indicated in the figure in green color. Figure 11 shows them in more details. The spectral region indicative of the emission from the glass substrate is marked by the red color and the Mo I emission lines with their relative intensities according to the NIST Atomic Spectra Data Base [9] are indicated by blue vertical lines.

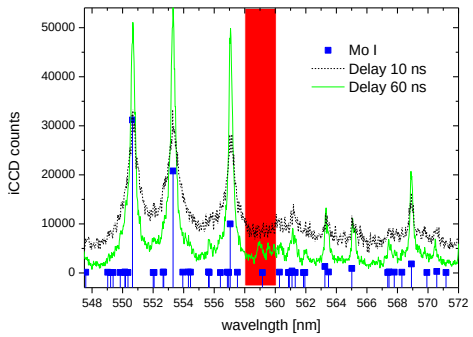

Figure 11: Laser initiated spectra of the interface plasma.

6 THERMAL ANNEALING

In order to clarify the role of the tensile stressed first layer, thermal annealing experiments were performed. For that, a box-type furnace under atmospheric conditions was used. The samples were entirely annealed for 20 minutes at 450 °C and cooled down slowly so that no additional stress could occur.
After the annealing the X-ray diffraction measurements as well as the determination of the ablation threshold were repeated. In Figure 12 the ratios of intrinsic stress and of laser ablation energy per volume before and after annealing are illustrated.

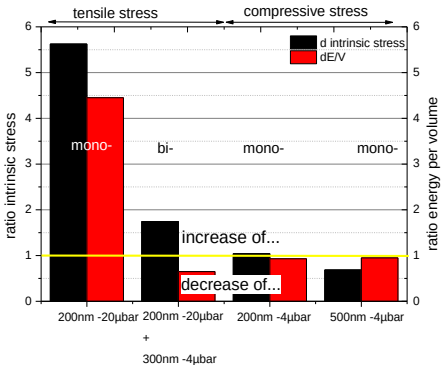

Figure 12: Ratio of intrinsic stress and ratio energy per volume is shown as function of the type of the stack before and after annealing.

As shown in Figure 12 for compressively stressed samples the intrinsic stress slightly decreases and an introduction of compressive stress for tensile stressed films occurs. This behavior is expected since it might be suggested that the compressively stressed layer slightly relax during thermal annealing. Subsequent cooling down to room temperature turns around the relaxing effect. Therefore, only little changes in the required ablation energy per volume could be determined.

In contrast to the compressively stressed samples show the tensile stressed ones a well distinctive increase of the intrinsic stress and thus an increase of the necessary energy per volume as well. This behavior is in good agreement with the expectation because the tensile stressed molybdenum layer expands less than glass do, which means the Mo would further expanded at the rising annealing temperature, it would relax at the temperature plateau and the following cooling down increase now the intrinsic stress. Thus the ratio of the required energy per volume increases and is > 1.

The following Figure 13 shows the behavior of all different samples thicknesses. It is obvious that the influence of thermal annealing is in generally very small for monolayer / compressively stressed samples whereas the tensile stressed layer systems are strongly influenced by thermal annealing. Moreover, it can be seen that with increasing thickness of the second layer at bilayer systems the influence of the annealing step decreases as it is indicated by the ratio of the required threshold energy per volume.

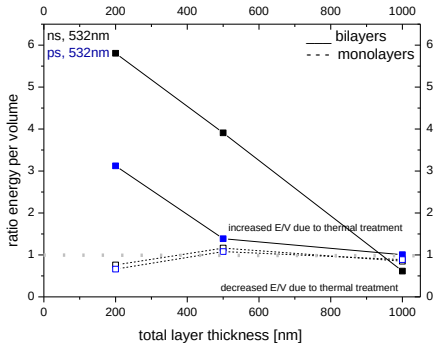

Figure 13: Ratio of the threshold energy per volume as function of the layer type and thickness is shown.

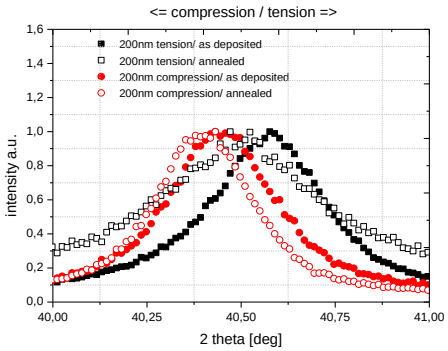

Figure 14: Comparison of the XRD-rocking curves of tensile and compressively stressed single layers before and after annealing.

The behavior of the intrinsic stress for the tensile and compressively stressed single layer before and after the annealing step are shown in Figure 14, as measured by XRD. These results support the behavior of both types of deposited layers mentioned above. It is obvious that all samples shown in Figure 14 exhibit larger compressive stresses after the thermal treatment.

7 ABLATION MODEL

Concluding the results of the previous sections, the post pulse ablation model for bilayer film side patterning can be described by the following four distinctive steps (illustrated in Fig. 15):

(1) In the first step the laser beam is absorbed at the surface of the 2nd layer of the stack and a heat flow to the molybdenum – glass interface takes place. Following thermal expansion of the entire stack leads to tensile stress close to this interface. This might suggest that the tensile stress reduces the adhesion to the substrate and thus enables low energies for ablation of the entire stack.

(2) The second step is dominated by melting and vaporization of the interfacial layer. Microscopic images indicate (data not shown here) that the substrate is molten at the irradiated spot. Time-resolved optical emission spectroscopy revealed the plasma generation which is leading to an increasing interfacial pressure supporting the delamination of the stack at the molybdenum/glass interface.

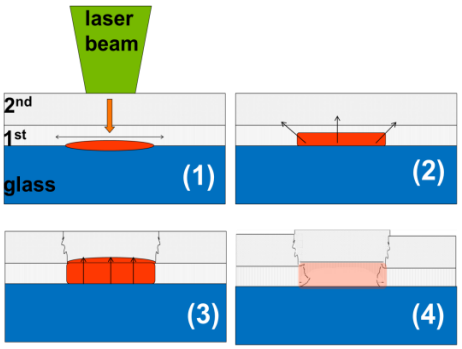

Figure 15: Principle of the film side post pulse ablation mechanism illustrated by four distinctive steps.

(3) After melting and vaporization of the interfacial layer an upward propagating pressure introduces the formation of radial cracks around the spot where the laser beam was absorbed.

(4) In the 4th step the interfacial pressure reaches a critical value and the entire molybdenum stack is spalled away. The critical value of the interfacial pressure depends on the mechanical properties of the deposited molybdenum as well as on the temporal behavior of the laser-matter interaction.

The following SEM images support the steps of this ablation mechanism. Figure 16(a) shows the onset of the cracking of the second layer with its typical circular shape. Above the cracking threshold a very clean crater is created and both molybdenum layers are removed, as shown in Figure 16(b). A more detailed view of the morphology of the crater walls of the spot is given in Figure 16(c). This image reveals the molten residuals of the tensile stressed 1st layer close to the substrate interface.

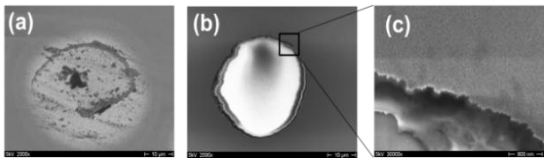

Figure 16: SEM images of different stages of the ablation of the molybdenum stack (image (a) & (b)), image (c) shows the morphology of the crater walls.

8 SUMMARY

In this study high-quality film side patterning of thin molybdenum films is demonstrated for laser pulse durations in the ns- and ps-range. It is shown that desirable patterning results are achieved by utilization of bilayer systems with a tensile stressed 1st layer. Furthermore, the bilayer stack enables good adhesion to the substrate as well as good electrical conductivity. Moreover, the role of the first layer was studied and it is suggested that this layer acts as intermediate layer and mediates mechanical stress. This behaviour leads to reduced compressive stress in the second layer, resulting in a decreased ablation threshold for ns- and ps-laser

pulse durations. The time resolved spectroscopy measurements indicate a thermal driven, most likely plasma assisted ablation mechanism. This laser process is a promising approach for flexible solar cells on low-cost substrates.

ACKNOWLEDGEMENTS

The authors would like to thank Bernd Szyszka for help- and fruitful discussions as well as the team of Jo Klaer (EI-3) for preparing the samples. This work was supported by the Federal Ministry of Education and Research (BMBF) and the state government of Berlin (SENBWF) in the frame work of the program "Spitzenforschung und Innovation in den Neuen Ländern" (grant no. 03IS2151C).

REFERENCES

[1] H.P. Huber, M. Englmaier, C. Hellwig, G. Heise, M. Kemnitzer, T. Kuznicki, C. Menhard, R. Brenning, A. Heiss, H. Vogt, J. Palm, Proc. 24th EU-PVSEC, Hamburg (2009).
[2] C. Schultz, M. Schüle, M. Richter, H.-U. Pahl, H. Endert, J. Bonse, I. Dirnstorfer, B. Rau, R. Schlatmann, V. Quaschning, F. Fink, B. Stegemann, Proc. 26th EU-PVSEC, Hamburg, 3AV.1.35 (2011), 2540.
[3] R. Witte, B. Frei, S. Schneeberger, Proc. 26th EU-PVSEC, Hamburg (2011)
[4] J.H. Scofield, A. Duda, D. Albin, Thin Solid Films, 260 (1995), 26.
[5] A.D. Compaan, I. Matulionis, S. Nakade, Final Technical Progress Report 12 April 1995 – 11 October 1997, NREL/SR-520-24842
[6] J.M. Liu, Opt. Lett., 7 (1982), 196.
[7] M. Richter, C. Schultz, J. Bonse, H.-U. Pahl, H. Endert, B. Stannowski, R. Schlatmann, V. Quaschning, B. Stegemann, F. Fink, Proc. 26th EU-PVSEC, Hamburg, 3DV.2.8 (2011), 2943.
[8] Y.G.Shen, Material Science and Engineering A 359 (2003), 158.
[9] http://www.nist.gov)